Available online at www.sciencedirect.com
ScienceDirect
Journal of Solid State Chemistry 180 (2007) 541–548
JOURNAL OF SOLID STATE CHEMISTRY
www.elsevier.com/locate/jssc

Composition and temperature dependent phase transitions in Co–W double perovskites, a synchrotron X-ray and neutron powder diffraction study

Qingdi Zhou[a], Brendan J. Kennedy[a,*], Margaret M. Elcombe[b]

[a]*Faculty of Science, School of Chemistry, The Centre for Structural Biology and Structural Chemistry, The University of Sydney, Chemistry Building (F11), Sydney, New South Wales 2006, Australia*
[b]*Bragg Institute, ANSTO, Menai, New South Wales 2234, Australia*

Received 1 September 2006; received in revised form 9 October 2006; accepted 25 October 2006
Available online 17 November 2006

Abstract

High-resolution synchrotron and neutron powder diffraction techniques were used to determine precise structures for the series of perovskite oxides $A_{2-x}Sr_xCoWO_6$ (A=Ca, or Ba, $0 \leqslant x \leqslant 2$). The studies demonstrated that the symmetry decreases as the average size of the A-site cation decreases with a sequential introduction of in-phase and out-of-phase tilting of the BO_6 octahedra. A cubic structure in $Fm\bar{3}m$ with rock-salt like ordering of the Co and W cations was formed for $Ba_{2-x}Sr_xCoWO_6$ with $x \sim < 1.4$. As the Sr content was increased, the materials became tetragonal in $I4/m$ and ultimately monoclinic in $P2_1/n$. A mixture of monoclinic and tetragonal phases occurs in Sr_2CoWO_6 at room temperature but this was purely monoclinic at 20 K.

Keywords: Double perovskites; Synchrotron and neutron diffraction

1. Introduction

Transition metal oxides with the rock-salt ordered double perovskite structure ($A_2B'B''O_6$) have been widely studied because of their interesting and technologically important magnetic and electric properties that include colossal magnetoresistance (CMR), ferroelectricity, high-temperature superconductivity, and exceptional ionic conductivity [1,2]. For example, the ordered double perovskite Sr_2FeMoO_6 exhibits a high magnetic transition temperature ($T_c \sim 400$ K) and pronounced CMR at room temperature, and these properties are superior to those displayed by the more widely studied manganese compounds [3]. Ferromagnetism with a T_c up to 458 K has been found in ceramic and thin film samples of Sr_2CrWO_6 [4]. Promising microwave dielectric properties have been observed in other tungsten containing double perovskite oxides A_2BWO_6 (A=Sr, Ba; B=Co, Ni, Zn) [5].

Over the preceding decade it has been established that the structural and magnetic properties of the ordered double perovskites $A_2B''B''O_6$ can be systematically tuned by altering the number of d-electrons of the B-site cation or the size of the cations. These substitutions can result in significant structural distortions that can, in turn, have a critical influence on the electric and magnetic properties of these oxides [4–6].

The earliest report of A_2CoWO_6 (A=Ba, Sr) double perovskites dates back to Fresia et al. who, in 1959, reported that Ba_2CoWO_6 was cubic and Sr_2CoWO_6 was tetragonal at room temperature [7]. These results have generally been confirmed by subsequent studies in [8,9]. However, there have been some conflicting reports, such as Zhao et al. who described both A_2CoWO_6 (A=Ba, Sr) as having cubic structures at room temperature [5]. Very recently Gateshki et al. described Sr_2CoWO_6 as undergoing a continuous phase transition from tetragonal $I4/m$ to cubic $Fm\bar{3}m$ near 430 °C [8], whilst Viola et al. [9] reported that Sr_2CoWO_6 becomes monoclinic upon cooling below 265 K. In all cases there is a rock-salt like ordering of the

*Corresponding author. Fax: +61 2 9351 3329.
E-mail address: kennedyb@chem.usyd.edu.au (B.J. Kennedy).

0022-4596/$ - see front matter © 2006 Elsevier Inc. All rights reserved.
doi:10.1016/j.jssc.2006.10.038

Co and W cations over the two octahedral sites with the changes in symmetry arising from different patterns of tilting of the octahedra.

In a recent comprehensive structural study of the double perovskites A_2NiWO_6 (A=Ba, Sr, Ca) we demonstrated that progressively increasing the effective size of the A-type cation by chemical substitution of the alkaline earth cation resulted in the sequence of structural phase transitions: $P2_1/n \xrightarrow{r_A=1.43\ \text{Å}} I4/m \xrightarrow{r_A=1.48\ \text{Å}} Fm\bar{3}m$, where r_A is the ionic radius of the A-type cation [10]. In order to demonstrate if the structural phases transition directly from $I4/m$ to $P2_1/n$ as seen in the series $A_{2-x}Sr_xNiWO_6$ [10] or goes via an $I2/m$ intermediate [11], a large number of oxides $A_{2-x}Sr_xCoWO_6$ (A=Ca, Ba) have been prepared and structurally characterized, using a combination of high resolution synchrotron X-ray and neutron powder diffraction methods. A preliminary account of the neutron diffraction studies was presented at the International Conference on Neutron Scattering in 2005 [12].

2. Experimental

A total of 24 samples in the series $A_{2-x}Sr_xCoWO_6$ (A=Ca, or Ba, $0 \leqslant x \leqslant 2$) were prepared by reaction of $CoWO_4$ with the appropriate amounts of the required alkaline earth metal carbonate ($BaCO_3$, 99.98% purity; $SrCO_3$, 99.9+%; $CaCO_3$ 99.995%;) at 900 °C/20 h and 1000 °C/40 h, with periodic regrinding. The samples were cooled in the furnace. The $CoWO_4$ was prepared by conventional solid-state methods from stoichiometric amounts of CoO and WO_3 at 900 °C/20 h.

Synchrotron X-ray diffraction data were collected on the Debye Scherrer diffractometer at the Australian National Beamline Facility, Beamline 20B at the Photon Factory, Tsukuba, Japan [13]. The samples were housed in 0.3 mm diameter capillaries that were rotated during the measurements. Data were recorded in the angular range $5° < 2\theta < 85°$, step size 0.01° using X-rays of wavelength 0.75049 Å with two Fuji Image plates being used as detector. Each image plate is 20×40 cm and covers 40° in 2θ. The wavelength was calibrated using Si 640c as a standard. Variable temperature data were collected, using a custom built furnace, at temperatures of up to 800 °C. All measurements were performed under vacuum to minimize air scatter.

Room- and variable-temperature neutron powder diffraction data were recorded in 0.05° steps in the range $10° < 2\theta < 150°$ using neutrons of wavelength 1.4925 Å on the High Resolution Powder Diffractometer (HRPD) at the HIFAR facility, ANSTO [14]. The samples were housed in vanadium containers throughout the measurements. Structural parameters were refined by the Rietveld method using the program RIETICA [15]. A pseudo-Voigt function was used to model the peaks. The background in the synchrotron diffraction patterns was estimated by linear interpolation between regions where there were no Bragg peaks, whereas a polynomial was used to fit the background in the neutron diffraction data.

3. Results and discussion

Highly crystalline samples of the various $A_{2-x}Sr_xCoWO_6$ (A=Ca, Ba) oxides were successfully synthesized using $CoWO_4$ as a precursor. The use of preformed $CoWO_4$ as a reagent allowed for accurate control of the B-site cation stoichiometry, such an approach previously being used to prepare other double perovskites including A_2NiWO_6 [10], A_2CrNbO_6 [16] and Sr_2YTaO_6 [17]. This method also has the additional significant advantages of allowing the reaction to occur at lower temperatures than described by previous workers [8,9] and, more importantly of minimizing the amount of secondary phase present in the final product. Heating of the samples at 1000 °C for even longer periods had no influence on the appearance of the diffraction patterns recorded using a Cu$K\alpha$ radiation. Comparison of our diffraction patterns with those described by Gateshki et al. [8] and Viola et al. [9] for Sr_2CoWO_6 revealed considerably less amounts of secondary phases such as $SrWO_4$ and Sr_2WO_5. Such phases are inevitably formed when a mixture of CoO and WO_3 is directly reacted with the appropriate alkaline earth cation. Tian et al. [18] have used sol–gel methods to avoid the formation of secondary phases in Sr_2CoWO_6.

3.1. Low and room temperature structures

The results obtained from the structural refinements using synchrotron data are listed in Table 1 and the diffraction patterns for the three single alkaline-earth containing oxides A_2CoWO_6 (A=Ba, Sr, or Ca) are presented in Fig. 1. The data for Sr_2CoWO_6 has a higher background as a consequence of fluorescence and subsequent absorption. These all show a strong (1 1 1)-type reflection near $2\theta = 9°$ indicative of rock-salt like ordering of the Co and W cations, with the patterns becoming progressively more complex as the size of the A-type cation was reduced from Ba to Ca. Fig. 2 summarize the composition dependence of the lattice parameters for the 24 samples at room temperature estimated from the synchrotron X-ray diffraction patterns. The patterns for the eight oxide $Ba_{2-x}Sr_xCoWO_6$ $x = 0$–1.4 (average A cation radii from 1.49 to 1.61 Å), could all be well fitted in a cubic model in $Fm\bar{3}m$, there being no indication of any peak splitting or asymmetry. All the observed diffraction peaks were accounted for with this model. The volume of the cell displayed an approximately linear reduction as the Sr content was increased in the series $Ba_{2-x}Sr_xCoWO_6$ (Fig. 2). Once the Sr content was increased above $x = 1.6$ ($r_A \sim 1.474$) some asymmetry became apparent in selected reflections, this increased as the Sr content was increased until well resolved splitting indicative of a tetragonal structure became apparent in the $x = 1.8$ ($r_A \sim 1.457$)

Table 1
Refined cell parameters, equivalent unit cell volume, and space group for the series A_2CoWO_6 at room temperature

Compounds	*A*-cation size (Å)[a]	*t*[b]	Fitness[c]	*a* (Å)	*b* (Å)	*c* (Å)	*β* (°)	Unit cell volume (Å^3)	Space group
Ca_2CoWO_6	1.34	0.957	0.936	5.4264 (1)	5.5778 (1)	7.7175 (1)	90.218 (1)	233.59 (1)	$P2_1/n$
$Ca_{1.8}Sr_{0.2}CoWO_6$	1.35	0.960	0.943	5.4513 (1)	5.5784 (1)	7.7456 (1)	90.150 (1)	235.54 (1)	$P2_1/n$
$Ca_{1.6}Sr_{0.4}CoWO_6$	1.36	0.964	0.950	5.4732 (1)	5.5752 (1)	7.7701 (2)	90.143 (2)	237.10 (1)	$P2_1/n$
$Ca_{1.4}Sr_{0.6}CoWO_6$[d]	1.37	0.967	0.957	5.4945 (1)	5.5686 (1)	7.7928 (2)	90.218 (3)	238.43 (3)	$P2_1/n$
$Ca_{1.2}Sr_{0.8}CoWO_6$	1.38	0.971	0.964	5.5284 (4)	5.5706 (4)	7.8241 (6)	90.310 (5)	240.95 (2)	$P2_1/n$
$CaSrCoWO_6$	1.39	0.974	0.971	5.5457 (2)	5.5740 (2)	7.8501 (4)	90.156 (4)	242.66 (2)	$P2_1/n$
$Ca_{0.8}Sr_{1.2}CoWO_6$	1.4	0.978	0.978	5.5587 (4)	5.5677 (3)	7.8818 (4)	90.182 (5)	243.93 (3)	$P2_1/n$
$Ca_{0.6}Sr_{1.4}CoWO_6$[d]	1.41	0.981	0.985	5.5700 (4)	5.5650 (4)	7.8923 (3)	90.190 (6)	244.64 (2)	$P2_1/n$
$Ca_{0.5}Sr_{1.5}CoWO_6$[d]	1.415	0.983	0.988	5.5761 (3)	5.5728 (3)	7.9014 (2)	90.167 (3)	245.53 (2)	$P2_1/n$
$Ca_{0.4}Sr_{1.6}CoWO_6$	1.42	0.985	0.992	5.5808 (3)	5.5792 (3)	7.9055 (2)	90.132 (2)	246.15 (1)	$P2_1/n$
$Ca_{0.3}Sr_{1.7}CoWO_6$	1.425	0.986	0.995	5.5899 (2)	5.5865 (2)	7.9185 (2)	90.141 (2)	247.28 (1)	$P2_1/n$
$Ca_{0.2}Sr_{1.8}CoWO_6$	1.43	0.988	0.999	5.5951 (2)	5.5912 (2)	7.9278 (2)	90.171 (2)	248.00 (1)	$P2_1/n$
Sr_2CoWO_6[e]	1.44	0.992	1.006	5.5854 (1)		7.9837 (1)		249.07 (1)	$I4/m$
$Ba_{0.1}Sr_{1.9}CoWO_6$	1.449	0.995	1.012	5.5952 (1)		7.9861 (1)		250.02 (1)	$I4/m$
$Ba_{0.2}Sr_{1.8}CoWO_6$	1.457	0.998	1.018	5.6047 (1)		7.9883 (1)		250.93 (1)	$I4/m$
$Ba_{0.4}Sr_{1.6}CoWO_6$	1.474	1.004	1.029	5.6240 (1)		7.9889 (3)		252.72 (1)	$I4/m$
$Ba_{0.6}Sr_{1.4}CoWO_6$	1.491	1.010	1.041	7.9870 (1)				509.51 (1)	$Fm3m$
$Ba_{0.8}Sr_{1.2}CoWO_6$	1.508	1.015	1.053	8.0116 (2)				514.23 (2)	$Fm3m$
$BaSrCoWO_6$	1.525	1.021	1.065	8.0299 (1)				517.76 (1)	$Fm3m$
$Ba_{1.2}Sr_{0.8}CoWO_6$	1.542	1.027	1.077	8.0473 (1)				521.14 (1)	$Fm3m$
$Ba_{1.4}Sr_{0.6}CoWO_6$	1.559	1.033	1.089	8.0649 (1)				524.57 (1)	$Fm3m$
$Ba_{1.6}Sr_{0.4}CoWO_6$	1.576	1.039	1.101	8.0855 (1)				528.60 (1)	$Fm3m$
$Ba_{1.8}Sr_{0.2}CoWO_6$	1.593	1.045	1.113	8.1004 (1)				531.52 (1)	$Fm3m$
Ba_2CoWO_6	1.61	1.051	1.124	8.1137 (1)				534.14 (1)	$Fm3m$

The numbers in parentheses are the estimated standard deviations.
[a] *A*-cation sive is the weighted average of the ionic radii for 12 coordinate cations as tabulated by Shannon [25].
[b] Tolerance factor given by $t = (r_A + r_O)/[\sqrt{2}(r_B + r_O)]$.
[c] Measure of fit given by $t = \sqrt{2}r_A/(r_B + r_O)$.
[d] Values obtained using data collected on a conventional diffractometer.
[e] Two phase $P2_1/n$ and $I4/m$ observed—see text for discussion.

sample. The patterns for the two oxides $x = 1.6$ and 1.8 were well fitted in the tetragonal space group $I4/m$. This space group has only out-of-phase tilting of the BO_6 octahedra and does not contain any additional superlattice reflections, over those due to the ordering of the Co and W cation. Whilst the fit to the synchrotron pattern for Sr_2CoWO_6 (r_A~1.44) appeared reasonable a number of small discrepancies were observed, a point we shall return to later. The X-ray diffraction pattern for Ca_2CoWO_6 showed well resolved splitting of the (cubic) 220 reflection indicative of monoclinic symmetry and the observation of weak X-point reflections, described in more detail below, in the pattern demonstrated the presence of in-phase tilts of the BO_6 octahedra. Consequently the pattern was fitted to a model in $P2_1/n$. This model proved adequate for the oxides $Ca_{2-x}Sr_xCoWO_6$ with $x = 0$–1.2 (r_A~1.34–1.40).

There are three features in Fig. 2 worthy of special comment. Firstly although the cell volume initially shows a linear dependence on the weighted average of the *A*-site cation radius for the cubic oxides, this relationship clearly breaks down for the smaller cations. The more rapid decrease in cell volume reflects the additional strain in these oxides that is presumably associated with the tilting of the octahedra. The second feature of note is the distinct discontinuity in the lattice parameters near r_A~1.44 (Sr_2CoWO_6) associated with the tetragonal ($I4/m$) to monoclinic ($P2_1/n$) transition. In Glazers [19] tilt notation this transition is $a^0a^0c^- \rightarrow a^+b^-b^-$ and involves the simultaneous introduction of in-phase (+ve) tilts about the [100] direction and the re-orientation of the out-of-phase (−ve) tilts from [001] to [011]. Such a transition must be first order [11]. Finally the oxides with r_A~1.42 are pseudo cubic ($a_p \approx b_p \approx c_p$) where the subscript refers to the equivalent primitive perovskite cell. The transition from cubic to tetragonal to pseudo-cubic to monoclinic is well illustrated by the composition dependence of the (cubic) 4 0 0 reflection near $2\theta = 22^\circ$, shown in Fig. 3. The formation of a pseudo-cubic phase is very similar to the behaviour seen in the analogous Ni series A_2NiWO_6 [10] and in other perovskites including $Ca_{1-x}Sr_xTiO_3$ [20,21].

In the above discussion we have implied that the pseudo cubic phase is in fact monoclinic in $P2_1/n$. Whilst such an assumption is likely to be valid based on our studies of the closely related A_2NiWO_6 series [10], it is not possible to confirm this choice of space group from the synchrotron diffraction patterns. To do this we employed high-resolution neutron diffraction methods, such data are more sensitive to the tilting of the octahedra, and therefore

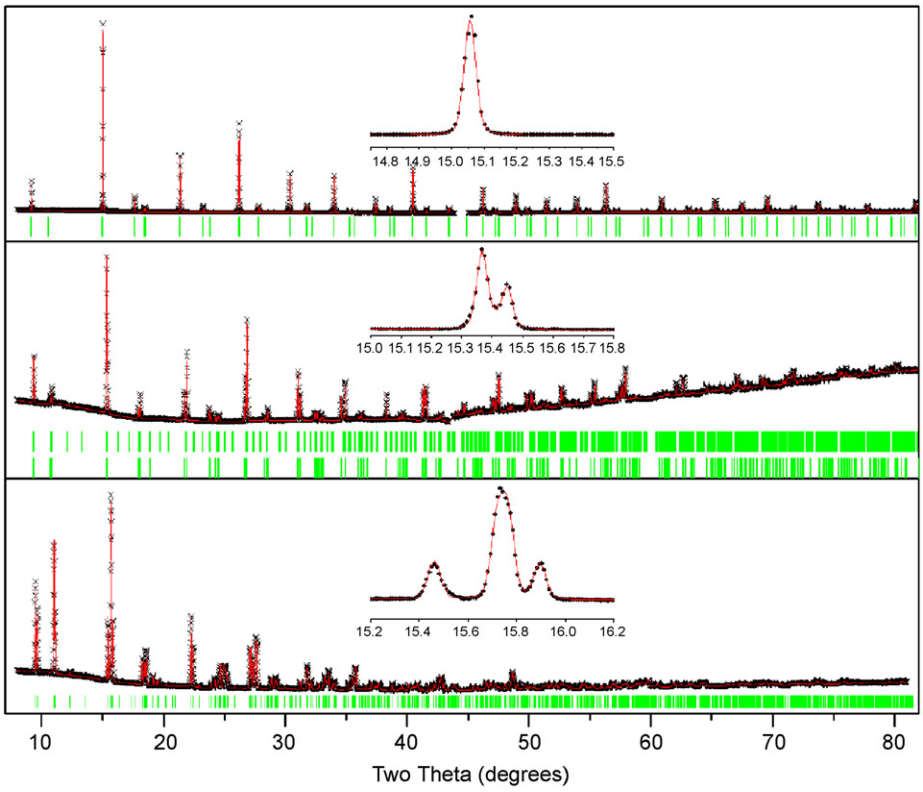

Fig. 1. Observed, calculated and difference synchrotron diffraction patterns for the three oxides A_2CoWO_6 (A=Ba, Sr and Ca). The markers show the positions of the allowed Bragg reflections. For Sr_2CoWO_6 the upper reflections are from the monoclinic phase and the lower from the tetragonal phase. The higher than typical background in this pattern is a consequence of absorption and fluorescence. The inserts in each pattern show the increased splitting of the, cubic, 2 2 0 reflection as the size of the A-cation is reduced.

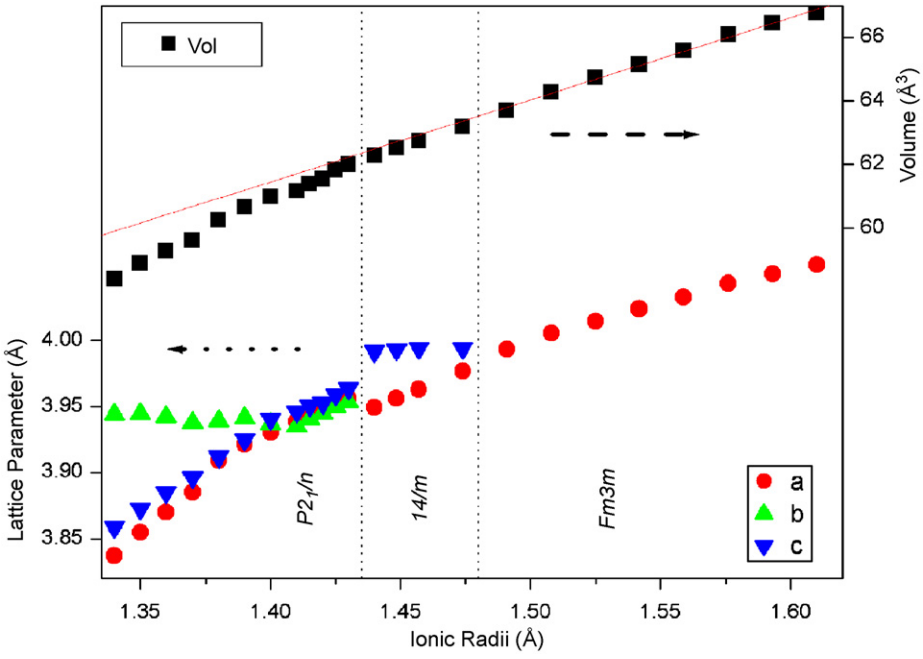

Fig. 2. Variation of the reduced lattice parameters and volumes with the average A cation radius for the series $A_{2-x}Sr_xCoWO_6$. The reduced lattice parameters are, for $P2_1/n$ $a' = \sqrt{2}a_p$, $b' = \sqrt{2}b_p$, $c' = 2c_p$ for $I4/m$, $a' = \sqrt{2}a_p$, $c' = 2c_p$ and for $Fm\bar{3}m$ $a' = 2a_p$.

allow the space group to be established. The additional, or superlattice, reflections that are observed in perovskites can be associated with particular modes in the Brillouin zone. For double perovskites the cation ordering results in the same additional R-point reflections as does out-of-phase tilting of the octahedra. The in-phase tilting is associated

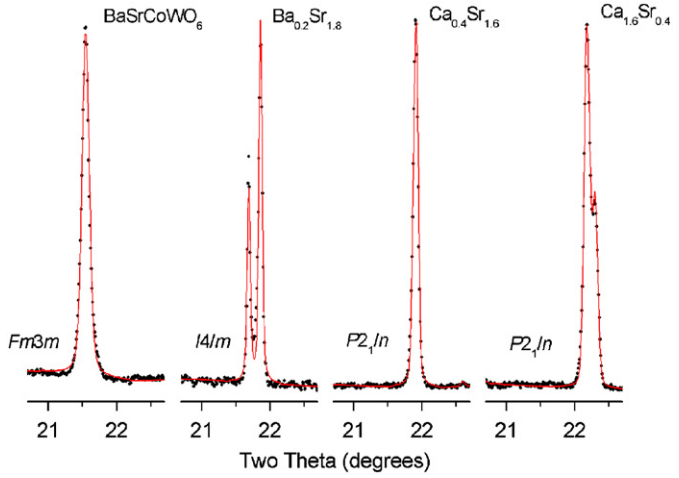

Fig. 3. Portions of the observed and calculated powder X-ray diffraction profiles for four members in the series $A_{2-x}Sr_xCoWO_6$, showing the formation of the pseudo-cubic phase near $r_A \sim 1.4$.

with an *M*-point mode while coupling of the out-of-phase tilts and the displacement of the A-type cation gives rise to *X*-point reflections. The interested reader is referred to Ref. [17] for more discussion on this.

High-resolution powder neutron diffraction patterns were collected for three samples $Ca_{2-x}Sr_xCoWO_6$ ($x = 1$, 1.5, 1.7, $r_A = 1.39$, 1.415, 1.425) at room temperature and for Sr_2CoWO_6 ($r_A = 1.44$) at 20 and 300 K. Table 2 lists selected structural parameters for Sr_2CoWO_6, the other results being tabulated elsewhere [12]. The three mixed *A*-cation oxides were selected since their synchrotron X-ray patterns did not show any obvious splitting of the Bragg reflections. Such splitting is clearly evident in both the synchrotron and neutron diffraction patterns of Sr_2CoWO_6. The neutron diffraction patterns of the three mixed Ca–Sr oxides reveal the presence of strong *M*-point reflections most noticeably the 1 2 0 and 1 2 2 reflections, observed near $2\theta \sim 35^\circ$ and 41° that demonstrate the presence of in-phase BO_6 tilting (Fig. 4). These together, with the *R*- and *X*-point reflections, show the oxides to be monoclinic in space group $P2_1/n$. The alternate monoclinic space group $I2/m$ that is observed in other double perovskites including Ba_2BiSbO_6 [22] and Ba_2BiLnO_6 [23] can be discounted from this evidence. It is important to recall that a $P2_1/n$ to $I2/m$ transition is allowed to be continuous and that these two phases should not co-exist. The hierarchal tree developed in the Group Theoretical analysis by Howard, Kennedy and Woodward [11] suggest a transition from $I4/m$ to $P2_1/n$ may involve an intermediate $I2/m$ phase but can also occur directly as found for A_2NiWO_6 [10]. The strength of the *M*-point superlattice reflections, apparent in Fig. 4, decreases with increasing Sr content as a consequence of a reduction in the magnitude of the octahedral tilting. The magnitude of the in-phase (+) tilts about the [1 0 0] direction and out-of-phase (−) tilts about the [0 1 1] direction, labelled φ and ψ, respectively, were estimated directly from the refined atomic coordinates as described previously [10]. The monoclinic $P2_1/n$ structure is presented in Fig. 5.

As noted above the fit to the synchrotron diffraction pattern for Sr_2CoWO_6 in the tetragonal space group $I4/m$, although reproducing the essential features of the pattern was not optimal. Consequently, we also examined this composition using powder neutron diffraction. Initially the neutron data was fitted using $I4/m$ however this yielded higher that expected *R* factors $R_p = 9.5$ and $R_{wp} = 12.7$ and more importantly did not reproduce all the observed reflections, see Fig. 6. Close scrutiny of the profile revealed weak intensity that could be ascribed to the *M*-point 1 2 0

Table 2
Structural parameters and displacement (Å^3) parameters for Sr_2CoWO_6 at room temperature

Space group	$P2_1/n$	$I4/m$
Sr		
x	0.0007 (7)	0
y	0.4909 (8)	0.5
z	0.2518 (15)	0.25
Biso	0.55 (5)	0.67 (5)
Co		
$x = y = z$	0	0
Biso	0.12 (27)	0.59 (29)
W		
$x = y$	0	0
z	0.5	0.5
Biso	0.67 (16)	−0.18 (13)
O1		
x	−0.0464 (6)	0
y	0.0005 (12)	0
z	0.2625 (11)	0.2598 (8)
Biso	0.52 (9)	1.11 (6)
O2		
x	0.2728 (14)	0.2911 (6)
y	0.2454 (14)	0.2250 (6)
z	0.0261 (12)	0
Biso	0.95 (19)	0.72 (4)
O3		
x	0.2405 (14)	
y	0.7243 (14)	
z	0.0205 (13)	
Biso	0.84 (16)	
a (Å)	5.6206 (2)	5.5793 (1)
b (Å)	5.5942 (2)	
c (Å)	7.9037 (3)	7.9796 (2)
β (°)	90.035 (6)	
Tilt angles[a]		
ϕ (°)	3.6	0
ψ (°)	7.6	7.4
Abundance (%)	51 (1)	49 (1)
R_w (%)	4.56	
R_{wp} (%)	5.56	

[a] φ refers to the magnitude of the in-phase (+) tilts about the [100] direction and ψ the out-of-phase (−) tilts about the [011] direction. These were calculated from the refined atomic coordinates.

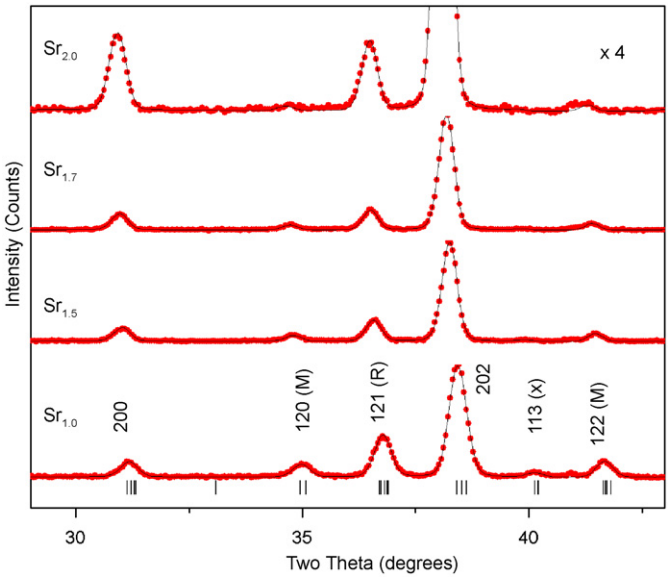

Fig. 4. Potion of the neutron patterns of four Sr containing samples illustrating the presence of both *R*- and *M*-point reflections in the patterns. While the *R*-point reflections can arise from either cation ordering or out-of-phase tilts the *M*-point reflections can only occur when in-phase tilts are present. The intensity scale for Sr_2CoWO_6 has been expanded to illustrate the very weak *M*-point reflections.

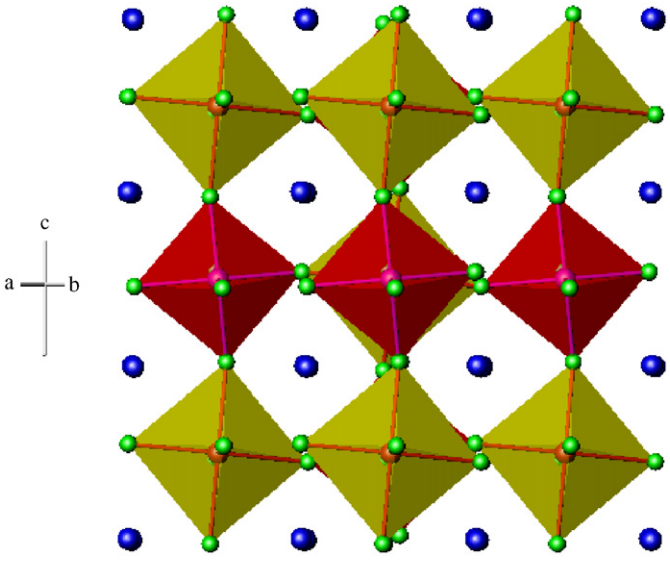

Fig. 5. Representation of the $P2_1/n$ monoclinic structure of the rock-salt ordered A_2CoWO_6 double perovskites showing the tilting of the octahedra. The *A*-type cations are represented by the small dark spheres.

and 1 2 2 reflections, showing the presence of in-phase tilts. However attempts to fit the profile in $P2_1/n$ were also viewed as unsuccessful ($R_p = 11.9$ and $R_{wp} = 17.0$). Given the first order nature of the $P2_1/n$ to $I4/m$ transition a model was developed containing both these phases and subsequence refinement of these structures resulted in a satisfactory fit to the observed neutron ($R_p = 4.6$ and $R_{wp} = 5.6$) and synchrotron ($R_p = 1.4$ and $R_{wp} = 2.0$) diffraction patterns. We suspect the failure of previous

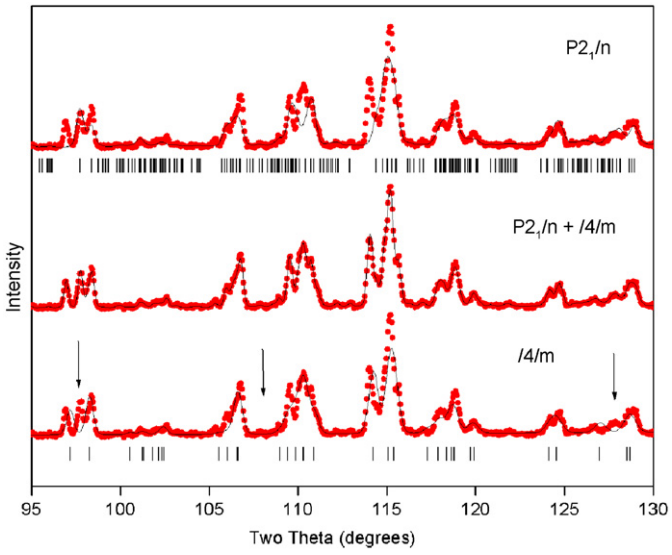

Fig. 6. Portions of the neutron diffraction pattern of Sr_2CoWO_6 fitted in single-phase $I4/m$ (bottom) and $P2_1/n$ (upper) models. The middle profiles show the successful fit using a two-phase $I4/m$ and $P2_1/n$ model. The arrows shows the diagonistic $P2_1/n$ reflections observed in the pattern.

workers to detect the co-existence of these two phases is due to either the quality of their diffraction data or, especially for the more recent studies [8,9], to difference in the preparative methods. The DSC measurements reported by Gateshki et al. [8] show a transition to occur very close to ambient temperature, with the heating and cooling cycles having slightly different transition temperatures. It is likely that the precise amounts of the two phases present will be dependent on the kinetics of the transition and consequently we would expect that this will be critically dependent on the thermal history of the sample. The powder neutron diffraction pattern of our sample of Sr_2CoWO_6 cooled to 20 K was well fitted in a single-phase monoclinic $P2_1/n$ model, demonstrating the co-existence of the two phases is an inherent consequence of the nature of the phase transition, rather than segregation due to sample inhomogeneities.

3.2. High temperature structures

The temperature dependence of the structures of $Ca_{0.2}Sr_{1.8}CoWO_6$ and $Ca_{0.4}Sr_{1.6}CoWO_6$ between room temperature and 800 °C were also investigated using synchrotron X-ray diffraction (Figs. 7 and 8). A first-order monoclinic to tetragonal transition was observed for $Ca_{0.2}Sr_{1.8}CoWO_6$ near ~300 °C and a continuous tetragonal to cubic transition close to ~625 °C. As was found in the composition dependent studies these are assigned to $P2_1/n \rightarrow I4/m \rightarrow Fm\bar{3}m$ transitions. Examination of the diffraction patterns for $Ca_{0.2}Sr_{1.8}CoWO_6$, Fig. 9, shows the relative intensity of the peaks derived from the cubic (4 4 0) reflection near $2\theta \sim 31^\circ$ to be reversed by the first order phase transition near 300 °C. This behaviour is diagnostic of the re-orientation of the octahedral tilts that

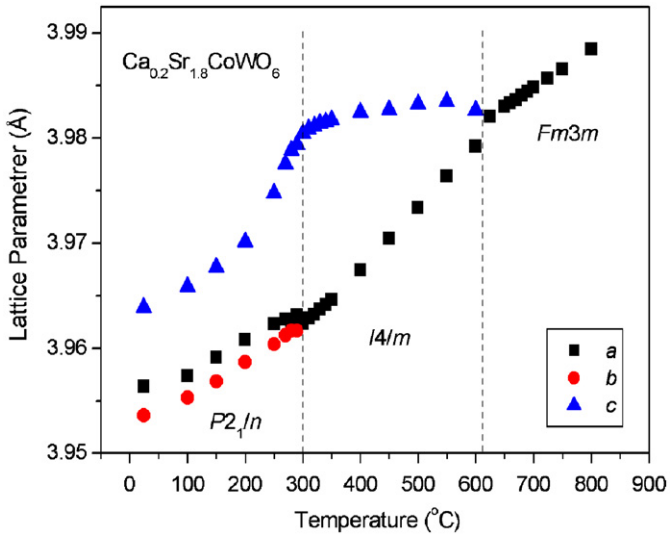

Fig. 7. Temperature dependence of the reduced lattice parameters for $Ca_{0.2}Sr_{1.8}CoWO_6$ deduced from refinements using synchrotron X-ray diffraction data. The reduced lattice parameters were calculated as for Fig. 2.

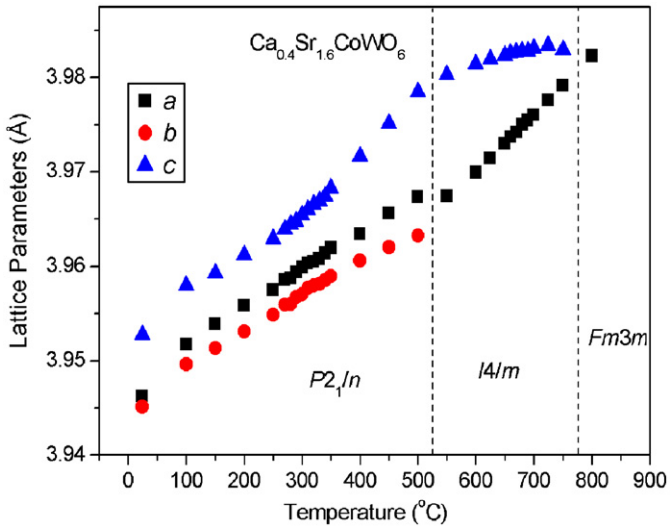

Fig. 8. Temperature dependence of the reduced lattice parameters for $Ca_{0.4}Sr_{1.6}CoWO_6$ deduced from refinements using synchrotron X-ray diffraction data. The reduced lattice parameters were calculated as for Fig. 2.

accompanies the phase transition from $I4/m$ ($a^0a^0c^-$) to $P2_1/n$ ($a^+b^-b^-$). The patterns recorded at or below 250 °C were well fitted with a single phase $P2_1/n$ model. Initially the pattern collected at 270 °C was also fitted to a single phase $P2_1/n$ model however this fit was not satisfactory. The 444 reflection near $2\theta \sim 38°$ is clearly not a single peak at temperatures below 310 °C, as required by $I4/m$ symmetry demonstrating this choice is also inappropriate. Consequently we fitted the patterns obtained between 260 and 300 °C using a two phase $I4/m$ and $P2_1/n$ model. This is the same model used to fit the room temperature neutron and synchrotron patterns for Sr_2CoWO_6 and resulted in excellent fits to the observed data (see Fig. 9). Heating the sample to above 625 °C resulted in the loss of any resolved peak splitting or asymmetry and the profiles were well fitted using the cubic $Fm\bar{3}m$ model. The results for $Ca_{0.4}Sr_{1.6}CoWO_6$ are very similar to those described for $Ca_{0.2}Sr_{1.8}CoWO_6$ save the transitions are shifted to higher temperatures; although in this case we found no evidence for the co-existence of the $I4/m$ and $P2_1/n$ phases, possibly as a consequence of the relatively course temperature intervals (25°) at this transition.

Whilst the present study has focussed on the effect of varying the size of the A-type cation comparison of these results with those for the analogous Ni compounds A_2NiWO_6 illustrates the influence of reducing the size of the B-site cation. The ionic radius of Ni^{2+} is 0.69 Å and of Co^{2+} 0.65 Å. For a given A-cation size the Co oxides will have a smaller tolerance factor and thus are expected to be more distorted. This is reflected in the high temperature phase transition behaviour of, for example, $Ca_{0.4}Sr_{1.6}CoWO_6$ and $Ca_{0.4}Sr_{1.6}NiWO_6$. In the Ni oxide the $P2_1/n$ to $I4/m$ transition is at ~300 °C whereas for the Co oxide it is near 550 °C. The corresponding $I4/m$ to $Fm\bar{3}m$ transition temperatures are ~700 and 800 °C, respectively. The smaller size of Co^{2+} cf. Ni^{2+} also accounts for the co-existence of the $P2_1/n$ and $I4/m$ phases in the present study of the Co oxide, whereas the Ni compound is single phase in $I4/m$ at room temperature, that is, the monoclinic phase persists to higher temperatures in Sr_2CoWO_6. These observations are in excellent agreement with the recent work of Gateshki et al. [11] on the series Sr_2MWO_6 (M=Co, Ni, Cu and Zn).

In conclusion, all the members of the series $A_{2-x}Sr_xCoWO_6$ (A=Ca, Ba) belong to the family of double perovskites where the two B-type cations Co and W adopt a rock-salt like ordered array of corner sharing BO_6 octahedra. The resulting voids are occupied by the larger A-type cations. As the effective size of the A-type cation decreases the BO_6 octahedra tilt to optimize A–O distances. The BO_6 tilting can also be very sensitive to temperature as seen, for example, in perovskite, $CaTiO_3$, itself [24]. This tilting results in the same sequence of phases at room temperature as seen in the analogous Ni series of oxides and is summarized as

$$P2_1/n \;\frac{r_A = 1.440\ \text{Å}}{r_A = 1.430\ \text{Å}} \rightarrow I4/m \;\frac{r_A = 1.491\ \text{Å}}{r_A = 1.480\ \text{Å}} \rightarrow Fm\bar{3}m,$$

where r_A is the weighted average ionic radius of the A-type cation, the upper numbers referring to the Co series and the lower numbers to the Ni series. We have found that in the sample of Sr_2CoWO_6 we prepared the monoclinic and tetragonal phases co-exist at room temperature, whereas the analogue Sr_2NiWO_6 was single phase and tetragonal. Variable temperature measurements on selected examples reveal the same sequence of phases.

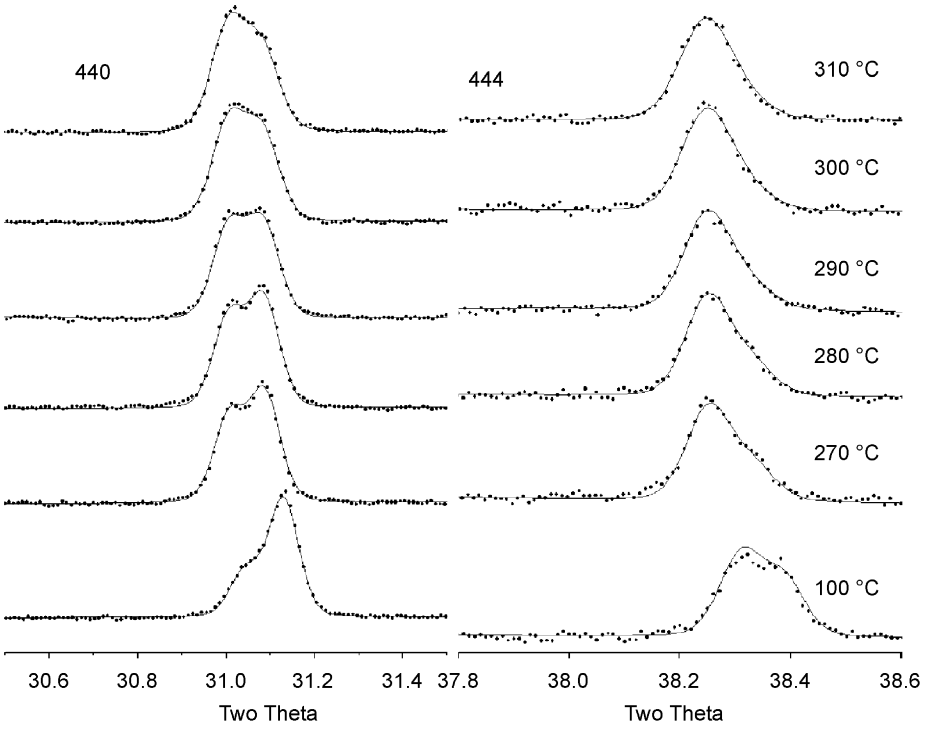

Fig. 9. Temperature dependence of the cubic 4 4 0 and 4 4 4 reflections in the synchrotron X-ray diffraction patterns of $Ca_{0.2}Sr_{1.8}CoWO_6$. Between 270 and 300 °C the fits were obtained assuming co-existence of the $I4/m$ and $P2_1/n$ phases.

Acknowledgments

This work was supported by a grant from the Australia Research Council. Synchrotron diffraction measurements were performed at the Australian National Beamline Facility with support from the Australian Synchrotron Research Program, which is funded by the Commonwealth of Australia under the Major National Research Facilities Program. The neutron diffraction measurements were supported by the Australian Institute of Nuclear Science and Engineering. The authors also gratefully acknowledge Dr. James Hester for assistance at the ANBF.

References

[1] R.H. Mitchell, Perovskites: Modern and Ancient, Almaz Press, Ontario, 2002.
[2] M.T. Anderson, K.B. Greenwood, G.A. Taylor, K.R. Poeppelmeir, Prog. Solid State Chem. 22 (1993) 197.
[3] K.-I. Kobayashi, T. Kimura, H. Sawada, K. Terakura, Y. Tokura, Nature 395 (1998) 677.
[4] J.B. Philipp, P. Majewski, L. Alff, A. Erb, R. Gross, T. Graf, M.S. Brandt, J. Simon, T. Walther, W. Mader, D. Topwal, D.D. Sarma, Phys. Rev. B 68 (2003) 144431.
[5] F. Zhao, Z.X. Yue, Z.L. Gui, L.T. Li, Jpn. J. Appl. Phys. 44 (2005) 8066.
[6] G. Popov, M. Greenblatt, M. Croft, Phys. Rev. B 67 (2003) 024406.
[7] E.J. Fresia, L. Katz, R. Ward, J. Am. Chem. Soc. 81 (1959) 4783.
[8] M. Gateshki, J.M. Igartua, E. Hernández-Bocanegra, J. Phys.: Condens. Matter 15 (2003) 6199.
[9] M.C. Viola, M.J. Martinez-Lope, J.A. Alonso, J.L. Martinez, J.M. De Paoli, S. Pagola, J.C. Pedregosa, M.T. Fernandez-Diaz, R.E. Carbonio, Chem. Mater. 15 (2003) 1655.
[10] Q. Zhou, B.J. Kennedy, C.J. Howard, M.M. Elcombe, A.J. Studer, Chem. Mater. 17 (2005) 5357.
[11] C.J. Howard, B.J. Kennedy, P.M. Woodward, Acta Crystallogr. B: Struct. Crystallogr. Cryst. Chem. B 59 (2003) 463.
[12] Q. Zhou, B.J. Kennedy, M.M. Elcombe, Physica B 385–386 (2006) 190–192.
[13] T.M. Sabine, B.J. Kennedy, R.F. Garrett, G.J. Foran, D.J. Cookson, J. Appl. Crystallogr. 28 (1995) 513.
[14] C.J. Howard, C.J. Ball, R.L. Davis, M.M. Elcombe, Aust. J. Phys. 36 (1983) 507.
[15] C.J. Howard, B.A. Hunter, A Computer Program for Rietveld Analysis of X-Ray and Neutron Powder Diffraction Patterns, Lucas Heights Research Laboratories, NSW, Australia, 1998, pp. 1–27.
[16] M.C.L. Cheah, B.J. Kennedy, R.L. Withers, M. Yonemura, T. Kamiyama, J. Solid State Chem. 179 (2006) 2487.
[17] C.J. Howard, P.W. Barnes, B.J. Kennedy, P.M. Woodward, Acta Cryst. B 61 (2005) 258.
[18] S.Z. Tian, J.C. Zhao, C.D. Qiao, X.L. Ji, B.Z. Jiang, Mat. Lett. 60 (2006) 2747.
[19] A.M. Glazer, Acta Crystallogr.B: Struct. Crystallogr. Cryst. Chem. B 28 (1972) 3384.
[20] C.J. Ball, B.D. Begg, D.J. Cookson, G.J. Thorogood, E.R. Vance, J. Solid State Chem. 139 (1998) 238.
[21] S. Quin, A.I. Becerro, F. Seifert, J. Gottsmann, J. Jiang, J. Mater. Chem 10 (2000) 1609.
[22] C.J. Howard, Z. Zhang, B.J. Kennedy, Acta Cryst. B 62 (2006) 537.
[23] R.B. Macquart, B.J. Kennedy, Chem. Mater. 17 (2005) 1905.
[24] B.J. Kennedy, C.J. Howard, B.C. Chakoumakos, J. Phys. C: Condens. Matter 11 (1999) 1479.
[25] R. Shannon, Acta Cryst. A 32 (1976) 751.